Pairwise mixture model for unmixing partial volume effect in multi-voxel MR spectroscopy of brain tumour patients

Olliverre, Nathan, Asad, Muhammad, Yang, Guang, Howe, Franklyn, Slabaugh, Gregory

Nathan Olliverre, Muhammad Asad, Guang Yang, Franklyn Howe, Gregory Slabaugh, "Pairwise mixture model for unmixing partial volume effect in multi-voxel MR spectroscopy of brain tumour patients," Proc. SPIE 10134, Medical Imaging 2017: Computer-Aided Diagnosis, 101341R (3 March 2017); doi: 10.1117/12.2255026

SPIE.

Event: SPIE Medical Imaging, 2017, Orlando, Florida, United States

Pairwise Mixture Model for Unmixing Partial Volume Effect in Multi-Voxel MR Spectroscopy of Brain Tumour Patients

Nathan Olliverre[1], Muhammad Asad[1], Guang Yang[2, 3, 4], Franklyn Howe[4], and Gregory Slabaugh[1]

[1]Department of Computer Science, City University of London, EC1V 0HB, London, United Kingdom
[2]Cardiovascular Biomedical Research Unit, Royal Brompton Hospital, SW3 6NP, London, United Kingdom
[3]National Heart & Lung Institute, Imperial College London, SW7 2AZ, London, United Kingdom
[4]Neuroscience Research Centre, St. Georges, University of London, SW17 0RE, London, United Kingdom

ABSTRACT

Multi-Voxel Magnetic Resonance Spectroscopy (MV-MRS) provides an important and insightful technique for the examination of the chemical composition of brain tissue, making it an attractive medical imaging modality for the examination of brain tumours. MRS, however, is affected by the issue of the Partial Volume Effect (PVE), where the signals of multiple tissue types can be found within a single voxel and provides an obstacle to the interpretation of the data. The PVE results from the low resolution achieved in MV-MRS images relating to the signal to noise ratio (SNR). To counteract PVE, this paper proposes a novel Pairwise Mixture Model (PMM), that extends a recently reported Signal Mixture Model (SMM) for representing the MV-MRS signal as normal, low or high grade tissue types. Inspired by Conditional Random Field (CRF) and its continuous variant the PMM incorporates the surrounding voxel neighbourhood into an optimisation problem, the solution of which provides an estimation to a set of coefficients. The values of the estimated coefficients represents the amount of each tissue type (normal, low or high) found within a voxel. These coefficients can then be visualised as a nosological rendering using a coloured grid representing the MV-MRS image overlaid on top of a structural image, such as a Magnetic Resonance Image (MRI). Experimental results show an accuracy of 92.69% in classifying patient tumours as either low or high grade compared against the histopathology for each patient. Compared to 91.96% achieved by the SMM, the proposed PMM method demonstrates the importance of incorporating spatial coherence into the estimation as well as its potential clinical usage.

Keywords: medical image analysis, magnetic resonance spectroscopy, partial volume effect, brain tumour, tissue classification, pairwise mixture model

1. INTRODUCTION

Brain tumours are the leading cause of cancer-related deaths in adolescents and young adults with there being over 78,000 cases of primary brain tumours diagnoses within any one year alone.[1] Patients diagnosed with brain tumours have a high probability of being given a poor prognosis, however survival rate and time of progression can be improved with the correct treatment.[2] Determining treatment, and the

Further author information: (Send correspondence to the lead author Nathan Olliverre at nathan.olliverre@city.ac.uk)

Medical Imaging 2017: Computer-Aided Diagnosis, edited by Samuel G. Armato III, Nicholas A. Petrick,
Proc. of SPIE Vol. 10134, 101341R · © 2017 SPIE · CCC code: 1605-7422/17/$18 · doi: 10.1117/12.2255026

correct location within the brain to apply treatment, is dependent on factors such as tumour grade, type and size.[3] Tasks performed manually, such as the segmentation of a brain lesion, for the aid in diagnosis of a brain tumour can be difficult and time consuming[4] with most errors in diagnosis occurring when a neuroradiologist is asked to determine the type of tumour.[5] The automation of tasks involved with diagnosis could help to increase the accuracy and reduce the time it takes for the application of treatment to a patient.

The World Health Organisation (WHO) guidelines classify brain tumours into four (4) grades: Grades I-IV, with GI and GII being deemed low grade tumours and GIII and GIV said to be high grade, malignant tumours. In accordance with The National Institute for Health and Care Excellence (NICE) guidelines[6] the standard procedure for brain tumour classification is a needle biopsy. A biopsy is an invasive procedure requiring the insertion of a hole within the skull to access the brain tissue sample, this can lead to risk of brain swelling and infection. The morbidity rate associated with a biopsy is reported to be a permanent 5%[7] and a mortality rate of between 0% and 1.7%[8] making it a considerably safe procedure, however the need for one can increase the time to diagnosis and be stressful for the patient. Medical imaging techniques such as Multi-Voxel Magnetic Resonance Spectroscopy (MV-MRS), also known as Chemical Shift Imaging (CSI) and Magnetic Resonance Spectroscopic Imaging (MRSI), provide a non-invasive method for the diagnosis of brain tumours.[9] However, MV-MRS produces new challenges, such as heterogeneous tissue signals found within each voxel, as well as how best to compare and classify the different resultant produced signals from one another.

Like Magnetic Resonance Imaging (MRI), MV-MRS is a based upon the principles of Nuclear Magnetic Resonance (NMR)[10] but whereas MRI uses the proton signals to produce detailed structural images,[11] MV-MRS uses the same proton signals to determine the quantity (in parts per million (ppm)) of various metabolites within cells of the brain.[12] MV-MRS can theoretically be applied to nearly any region of the human body but has found to be most useful, clinically, in the imaging of the brain, this is in no small part thanks to the homogeneity in the structure of brain tissue. When imaging the brain MV-MRS typically uses Hydrogen (^{1}H) protons due to the high levels found *in vivo* as well as the ^{1}H protons sensitivity to magnetic manipulation. From an MV-MRS scan the resultant metabolite levels measured can be interpolated and displayed as a spectrum of varying peaks (resonances) along an x-axis labelled in ppm. The understanding of the more prevalent metabolites e.g. N-Acetylaspartate Acid (NAA), Choline (Cho) and Lipids, can help to determine the biochemical composition of the tissue being examined. Taking into account that it has been shown that the grade of a tumour is directly correlated with the corresponding MRS signal[13] e.g. a decrease in levels of NAA indicates neuronal loss or damage, modern pattern recognition techniques can be applied so that models may be formulated from these signals. The models created can then be used for tissue characterisation.

Due to the heterogeneity of the tissue that can be found in any voxel from an MV-MRS image, as well as the imprecision of the delineation of tumour tissue grade boundaries, manual interpretation of MV-MRS imaging is difficult. The difficulty in manual MV-MRS classification is then compounded by the time consuming nature of the diagnosis process which is worsened, still, when dealing with large datasets. To resolve the issue of the difficulty in understanding MV-MRS imaging, and the length of time it takes for diagnosis, automated pattern recognition methods have been applied to MV-MRS imaging for their use in Computer Aided Diagnosis (CAD). Methods have involved the use of nosological imaging to compile and outline the various metabolite levels of important chemicals used as markers for certain tumours in the brain.[14,15] Other have been used to highlight the boundaries of tumours to facilitate in the understanding of tumour growth and direction of said growth.[16,17] The appearance of an MV-MRS image, as a digital signal, provides the opportunity to utilise modern pattern recognition methods in an attempt to classify brain tumours from MRS images. To optimise the process, dimensionality reduction is required to scale the high spatiality of the MV-MRS signals to that of a lower representation, with a minimal loss of the relationship between values in a given signal. Popular dimensionality reduction

techniques prior to pattern recognition in CAD systems have been applied to MV-MRS datasets such as Principal Component Analysis (PCA)[18] and Independent Component Analysis (ICA).[17] Techniques like Laplacian Eigenmaps (LE)[4,19,20] and Non-Negative Matrix Factorisation (NNMF)[21] have also been applied to MV-MRS datasets for CAD systems.

Pattern recognition methods for CAD of MRS images have taken the form of semi-supervised[22] and unsupervised[4] approaches, most have required the creation of a set of models from the MV-MRS dataset they are working on for accurate interpretation of a new signal. The creation of models from MV-MRS signals requires correctly labelled prior information, therefore the previous work assumes homogeneity within the labelled data and that of the test data. To determine, at a granular voxel level, the correct grading of a brain tumour using MV-MRS means overcoming the critical challenge of the Partial Volume Effect (PVE). The PVE in MV-MRS is the diminution of the differentiation between multiple tissue types within a single voxel caused by coarse resolution in the imaging process. One way to lessen the PVE is to reduce the slice thickness of each scan, however with MV-MRS a larger voxel size is used, thus weakening the resolution (especially when compared to that of structural MRI), in order to boost the signal to noise ratio (SNR) and to keep a reasonable acquisition time. This lack of contrast in the tissues results in what appears as a mixture of multiple tissue types in each voxel observed. Within MV-MRS brain images, possible tissues can include normal/healthy brain tissue such as Cerebral Spinal Fluid (CSF), water tissue and fat tissue, necrotic tissue (dead tissue) and tumour tissue. Any tumour tissue observed may also be a mixture of the various grades of tumour (GI - GIV) providing an even greater challenge to overcome in voxel tissue classification. To resolve the PVE issue, work using estimations of the mixture of tissue types per voxel have included using a supervised derivation of model spectra for the sub-spectral analysis of a new input image.[23] Other attempts have included spatial constraints so as to add previous knowledge on the shape of tumour/lesion boundaries to improve the mixture estimations.[14]

The method proposed in[18] describes a supervised Signal Mixture Model (SMM) that aims to resolve the Partial Volume Effect (PVE) by differentiating MV-MRS images into three classification grades of either normal, low or high grade brain tissue types (low representing infiltrative tumour tissue and high necrotic tumour tissue). The SMM framework (Figure 1) is a two framework system, the first, the Training framework, has the SMM learn the tissue models using a histologically labelled Single-Voxel Magnetic Resonance Spectroscopy (SV-MRS) dataset. The histological labels achieved by directing a scan specifically onto a homogeneous region of tissue determined by specialists. Principal Component Analysis (PCA) is then applied to the dataset to produce a mean and a set of eigenvectors per tissue grade. The second framework, the Prediction framework, solves an optimisation problem, one of the SMM against a new input MV-MRS signal using weight coefficients, the value of each weight coefficient representing the prevalence of a respective tumour tissue grade within the MV-MRS signal. Taking the values of the weight coefficients, RGB probability heatmap visualisations (heatmaps) can be formulated, providing a descriptive and intuitive manner with which to help physicians with tumour analysis. The heatmaps are adapted from work on RGB heatmaps[23] which took inspiration from nosological images,[24] where, with nosological images, every voxel from an MV-MRS image is analysed and assigned to a histopathological class. The continuation of RGB heatmaps relates the colour to that of the type of tissue, and any possible combinations of tissue, to represent the mixture found, per voxel.

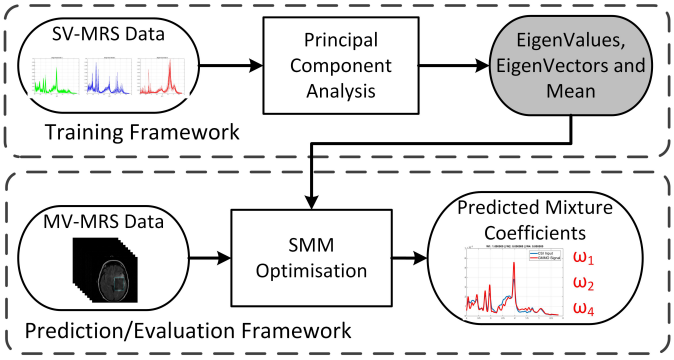

Figure 1. Diagram of the Signal Mixture Model

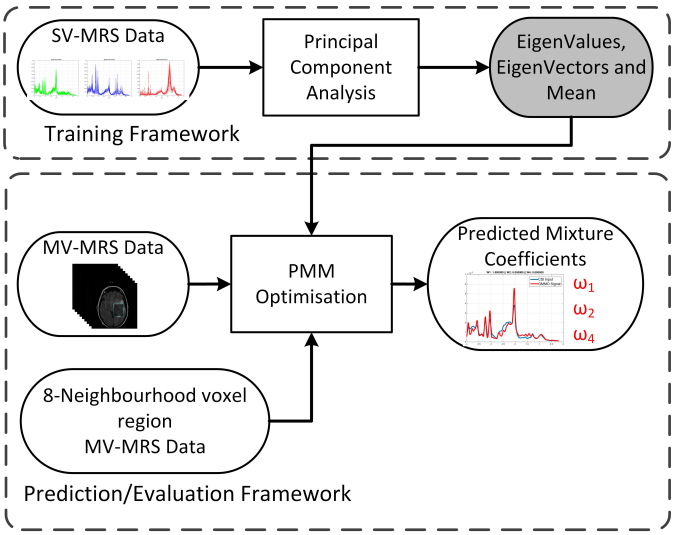

Figure 2. Diagram of the Pairwise Mixture Model

The accuracy of any classification using pattern recognition methods in medical imaging, is dependant on the precision of both, the models created for the various tissue types found within the area being assessed, and the medical images themselves. Within the SMM, model accuracy is constrained by imperfect definition of the individual tissue type signals[25,26] and the overlap in the characteristics of the different tissues.[27] MV-MRS image correctness is challenging due to the SNR,[28] distortion[26] and potential artefacts within signals.[9,29] The SMM estimates the signal mixture per voxel and makes the assumption of an independence in tissue type signals as well as excellent SNR with little to no distortion. The estimation per voxel, is performed in the SMM Prediction framework, the optimisation problem is solved over the whole MV-MRS input image and thus is calculated without consideration for the information provided by the values of surrounding voxels. Previous work[25,30] has shown there to be a considered delineation between that of tumour tissue and other tissue within the brain. Taking the contrast into account as well as the acceptance of the probability for distortion and artefact within an MV-MRS image, a smoothing process over all voxels relative to position within an image can help to provide better defined boundaries and clearer detail. Recent work including[31] and[32] has detailed methods that perform smoothing using

spatial awareness to an image; however the images used in the methods are binary while there are three labels within the SMM. Work on smoothing[33] describes a Conditional Random Field(s) (CRF(s)) with alpha expansion which can be applied to images with more than two labels. By taking the SMM as a representation, the performing of a smoothing using the spatial awareness of surrounding voxels could help to increase the accuracy of the model.

By combining the method of the SMM with neighbourhood information inspired by a CRF, a new spatially aware model can be constructed. By incorporating the surrounding signal information to every voxel, this "smoothing" could assist in overcoming the issues in classification. Interpreting the SMM model of an input signal as a unary term and incorporating a pairwise term to include the information of the neighbouring voxels a new model can be derived. This new model (named PMM for Pairwise Mixture Model) can take into account the knowledge of the influence that the higher the frequency of a certain tissue in a region the more likely that there is homogeneity. The PMM then uses the information from the surrounding neighbourhood to repress or encourage the prediction of the different tissue types at each voxel (Figure 2).

This is the first study to put forward a model incorporating the surrounding voxel information for tackling the issue of the PVE aimed at brain tumour characterisation, per voxel, for the use in CAD. The results show an increase in the total classification accuracy of the proposed model over the previous method with and the possible benefit of incorporating neighbouring information for smoothing to benefit a CAD systems in medical imaging.

2. METHOD

Taking influence from the theory of CRFs and their continuous variant, we note that neighbouring samples can impart influence onto each other,[34] providing a model with locational context. By encoding possible relationships between surrounding nodes and expanding on the framework from the SMM (Figure 1), the proposed Pairwise Mixture Model, differentiates brain tissue, per voxel, as a combination of Normal grade (n), Low (infiltrative) grade (l) and High (necrotic) grade (h). An MV-MRS signal can be defined as $x(t)$ with the signal modelled by the PMM as $s(t)$ where t represents the frequency of metabolites in parts per million (ppm). Taking a dataset of various tissue grade types, obtained from, carefully placed, SV-MRS scans over homogeneous tissue type regions, the tissue grade models are defined $(i \in n,l,h)$. Each tissue grade model is expressed as a mean signal as well as the variation around the mean, calculated from applying PCA to the subset of SV-MRS dataset relating to a specific grade, as defined by the model:

$$m_i(t) = \mu_i(t) + \sum_{k=1}^{K} \alpha_{ik} e_{ik}(t), \tag{1}$$

where u_i is the mean signal, α_i and e_i respectively are the alpha weight coefficients and eigenvectors which encode the variation around the mean signal, with K representing the number of eigenvectors determined for model i.

If a tissue type represented by a voxel within a MV-MRS image were to be homogeneous, and taking the signal models defined by PMM to be accurate representations, then it should be expected that the voxel signal be fully modelled by the PMM. Using MV-MRS for brain tumour classification and delineation requires the Partial Volume Effect (PVE) be overcome, studies such as[14,18,23] have presented ways with which to deal with the PVE in analysing MRS scans. Due to the PVE the expectation of tissue homogeneity from every input voxel is not possible. Instead a heterogeneous mix of various tissue type is expected to be found. To model this mixture within every voxel, an input signal is defined as a superposition of each tissue grade model $(m_n(t), m_l(t), m_h(t))$:

$$s(t) = w_n m_n(t) + w_l m_l(t) + w_h m_h(t), \tag{2}$$

where w_i are the weight coefficients representing the prevalence of the respective tissue type found within the input signal. The weight coefficients are thus constrained by the following:

$$w_n + w_l + w_h = 1 \text{ and } 0 \leq w_n \leq 1,\ 0 \leq w_l \leq 1,\ 0 \leq w_h \leq 1. \tag{3}$$

Taking the mixture model created $(s(t))$ and given a new MV-MRS signal $(x(t))$ an optimisation problem can be created to best fit $s(t)$ to $x(t)$ so as to calculate the weight and alpha coefficients $(w_n, w_l, w_h, \alpha_{nk}, \alpha_{lk}, \alpha_{hk})$ $\forall k$. Mathematically the optimisation described is formulated as:

$$E = \int [x(t) - s(t)]^2 dt. \tag{4}$$

The optimisation problem in Equation (4) has no spatial context so does not take into account any information provided by the possible influence that surrounding signals may have on each other. Taking inspiration from the energy minimisation problem of CRF, we incorporate a pairwise term describing the difference between neighbouring voxels. This can be modelled as:

$$E = \int [x(t) - s(t)]^2 dt + \int [\sum_j s(t) - s_j(t)]^2 dt, \tag{5}$$

$$\text{where } j \text{ are the available surrounding model signals of s(t).} \tag{6}$$

Equation (5) describes the energy for minimisation of the difference between the input signal $x(t)$ to the attempted model $s(t)$ and the model signal's closeness to the surrounding voxels model signals $s_j(t)$. The latter term of Equation (5) defining the difference between each voxel's model and its neighbourhood by the summed difference of itself and over its surrounding j voxels.

Taking Equation (5), gradient descent is used to optimise the energy where the values for the weight and alpha coefficients are calculated iteratively from the initial solution by moving each value in the direction of the negative gradient. At each iteration the weights are normalised to adhere to the constraints of Equation (3). Taking the partial derivative of Equation (5) with relation to the weight parameters we get:

$$\frac{\partial t}{\partial w_i} = -2 \int \Omega m_i(t) dt + \int \sum_n \frac{\partial}{\partial w_i} [s(t) - s_n(t)]^2 \mathrm{d}t, \tag{7}$$

$$\text{where } \Omega = x(t) - \sum_i w_i \left(\mu_i(t) + \sum_{k=1}^{K_i} \alpha_{ik} e_{ik}(t) \right), \tag{8}$$

$$\text{and } \frac{\partial}{\partial w_i} [s(t) - s_n(t)]^2 = -2 \int \Phi m_i(t) \mathrm{d}t, \tag{9}$$

$$\text{where } \Phi = \sum_n s_n(t) - s_i(t). \tag{10}$$

Taking the partial derivative of Equation (5) with relation to the alpha parameters we get:

$$\frac{\partial E}{\partial \alpha_{ik}} = -2 \int \Omega w_i e_{iK}(t) dt + \int \sum_n \frac{\partial}{\partial \alpha_{ik}} [s(t) - s_n(t)]^2 \mathrm{d}t, \tag{11}$$

$$\text{where } \Omega = x(t) - \sum_i w_i \left(\mu_i(t) + \sum_{k=1}^{K_i} \alpha_{ik} e_{ik}(t) \right), \tag{12}$$

$$\text{and } \frac{\partial}{\partial \alpha_{ik}} [s(t) - s_n(t)]^2 = -2 \int \Phi w_i e_{ik}(t), \tag{13}$$

$$\text{where } \Phi = \sum_n s_n(t) - s_i(t). \tag{14}$$

At initialisation, an MV-MRS signal $x(t)$ is projected onto the three signal models, forming a fully projected signal. The initial projection is then used as an estimate for the weight and alpha coefficients. From this initial projection the residual r_i from each tissue grade i is taken; which describes the error in representing a signal by the PMM. Each weight coefficient is initialised with:

$$w_i = 1 - \frac{r_i}{r}, \quad \text{where} \quad r = \sum_j r_j. \tag{15}$$

At the end of each iteration the weights are then normalised to adhere to the constraints of Equation (3). Taking the fully derived PMM, the training framework uses a SV-MRS dataset to derive the base models, before being tested on a MV-MRS dataset within the prediction framework Figure 2.

3. EXPERIMENTS AND RESULTS

The training SV-MRS and test MV-MRS datasets, applied to the PMM, were acquired using a GE Signa Horizon 1.5T MR system with a Repetition Time (TR) and a short Echo Time (TE) of 2000ms and 30ms respectively. A Point-Resolved spectroscopic sequence protocol was used to acquire the SV-MRS dataset with a PROBE-SI protocol for the MV-MRS data. The composition of the SV-MRS data was 137 samples, of those 79 were classified as normal tissue, 23 as GII, 10 as GIII and 25 GIV. The positioning for every scan captured in the SV-MRS dataset was determined by expert, analytical decision according to post-Gd contrast T1w, T2w and FLAIR structural contrast images on a homogeneous representative tumour region alongside the relevant histopathical information. Within the training data acquired there was a heterogeneity of MRS characteristics represented. The labels/ground truths for the SV-MRS data were achieved via the diagnosis of a biopsy by a practised physician in which the clinical, radiological and histopathological information of each patient was incorporated to the diagnosis as well. The MV-MRS data was acquired from 31 patients with the ground truth (GT), histological diagnosis, determining 12 patients to be graded as GII, 7 as GIII and 12 as GIV. The GT for the MV-MRS data was acquired through the histological examination of the core of the tumour, determined by a physician, via biopsy of the patients.

The SV-MRS data was used to train and build the PMM, where Grade n included normal tissue samples, Grade l included GII and Grade h included GIV, which was then validated and tested using the MV-MRS data. Due to the heterogeneous characteristics of tumours, the classification of GIII tumours posed a challenge. The GIII challenge was due to the signal for GIII tumour tissue having close similarities to, and sometimes being indistinguishable from the signal from both GII and GIV tumour tissue. The PMM was, therefore, trained on two separate datasets, one which included the SV-MRS GIII data and one without, with each trained model tested individually on the same test dataset. After experimentation with different sizes (0, 2, 4 and 8, with 0 being used as a control) an 8-neighbourhood was selected for use after providing the most accurate results. For voxels at a boundary the neighbourhood was taken for all possible surrounding voxels available with no null values or normal tissue signals used to propagate the neighbourhood. The results displayed in Table 1 include both sets of tests, those with the SV-MRS GIII data included in the training of the PMM, high grade, base model and those without the SV-MRS GIII data included.

The predicted grading for each patient from the MV-MRS dataset used by the PMM was determined to be the highest grade tissue found, the highest tissue grade was defined as the tissue corresponding to the coefficient w with the maximum value.

$$\text{patient}_i = \max_{i \in \{n,l,h\}}(w_i), \tag{16}$$

where patient_i is the predicted grading for a given patient.

Table 1. Results for PMM and SMM on 31 patient dataset

Model	Grade L	Grade H		GIII Included	Average Accuracy	Balanced Error Rate
	GII	GIII + GIV	GIV			
	12	7 + 12	12			
SMM	83.33%	84.21%	91.67%	Yes	86.40%	0.1360
PMM	**91.67%**	**89.47%**	**91.67%**	**Yes**	**90.94%**	**0.0906**
SMM	91.67%	84.21%	100%	No	91.96%	0.0804
PMM	**83.33%**	**94.74%**	**100%**	**No**	**92.69%**	**0.0731**

From the results in Table 1 the PMM can be seen to have the higher accuracy overall showing an improvement over the SMM in successfully classifying an increased number of lower grade tumours when not including the GIII samples in the training dataset. The PMM also shows a lower Balanced Error Rate (BER) against that of the SMM in both including and not including the GIII training data. The case of higher accuracy within the lower grade tumour set (GII) can be possibly attributed to the smoothing effect from neighbouring voxels, reducing any voxels predicted to have a higher grade tissue to that of a lower grade and thus reducing the weighting of high grade tumour and increasing the weighting of low grade making the classification of the patient class lower. Looking at the training data for both methods, when the GIII training data was not included both methods produced higher accuracy results with the PMM having a higher average accuracy and lower BER. When looking at each method individually it can be seen that there was an increase in accuracy for the PMM over the SMM in classifying the GIII + GIV tumour grade set when including the GIII training data. Without the GIII data included in training the PMM had difficulty classifying lower grade scans correctly, compared to the SMM, with the GIII training data included, the PMM outperformed the SMM. It is difficult to analyse the results from experimentation in too much detail due to the lack of a histological label per voxel. The limited amount of data available for testing also limits the strength of any conclusions made, this makes the case for future work acquiring and utilising larger datasets which will enable more detailed understanding of the PMMs advantages/disadvantages and provide opportunity to make stronger conclusions.

From the fitting performed by the PMM the resultant weight coefficients from a new MV-MRS scan, relates to the probability of classifying the input into one of the three tissue grades (normal, low or high grade tumour, brain tissue). Using the mixture coefficients, RGB probability heatmaps can be produced by overlaying the resultant values for each coefficient, for each tumour grade, onto the related MV-MRS brain image. Each heatmap relates to the likelihood of the corresponding regions concentration of all three types of brain tissue, here each colour green, blue and red corresponds to each tissue type normal, low grade and high grade respectively in the related voxel of a MV-MRS image. In a given heatmap the 24-bit RGB representation is calculated by the values for each coefficient for each brain tissue type in each MV-MRS voxel. The higher the mixture coefficient value the more intense the related colour. These heatmaps can then be placed upon a structural MRI image of the patient creating heatmap graphs (see Figures 3 - 7) that can aid in human interpretation of the data.

Comparing the resultant heatmaps from both the PMM and the SMM, using the same testing dataset, seen in Figures 3 - 7, presents a clearer method to understand the difference between PMM and SMM. In Figure 7 it can be seen the effect of the spatial context has on the scans with more defined areas of the scan from the PMM (left) compared to the slightly less defined regions from the SMM (right). Looking at Figure 5 it is easy to notice the more bounded regions, however whether the regions of low grade tumour tissue that has become distinct are correct or not is debatable, without a per voxel histological label available.

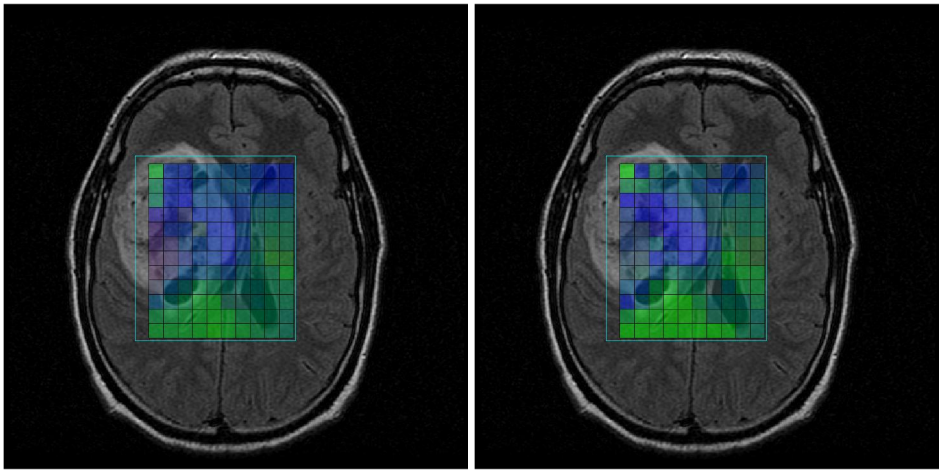

Figure 3. Results show a Grade III patient scan (h) which is correctly classified by PMM (left) due to the neighbourhood information, but misclassified by SMM (right). However there does show an increase in two voxels misclassifying tumour tissue as strongly normal tissue in the PMM scan.

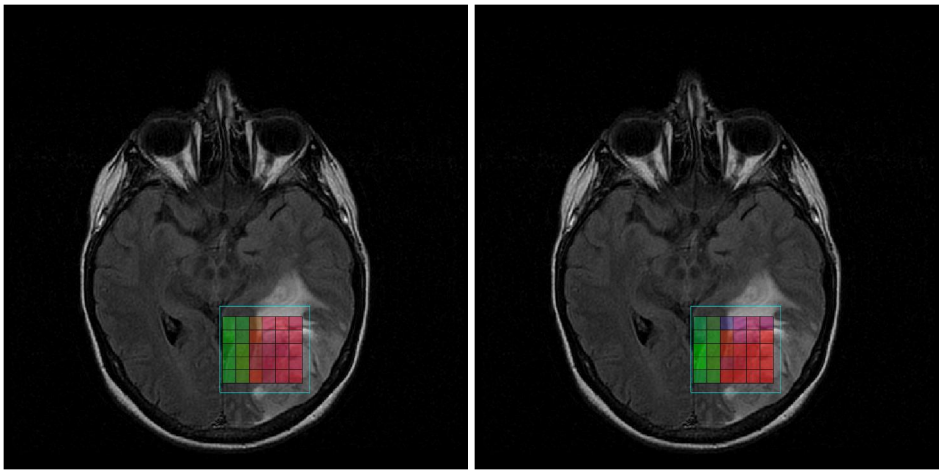

Figure 4. Results show the influence from surrounding voxels in the PMM (left) which helps to create more defined boundaries (which may be helpful in determining the centre of a tumour), between structures within the scans when compared to that of the SMM (right). Boundary definition is difficult due to the limited precision from MV-MRS images in places such as where voxels straddle a boundary, this may mean that the tissue within the voxel, which was smoothed, was in fact low grade tumour tissue. From manual analysis of the spectra the core of the tumour is known to be high grade and the boundary to be a mix of high grade tumour with normal tissue making the results from the PMM more accurate than that from the SMM.

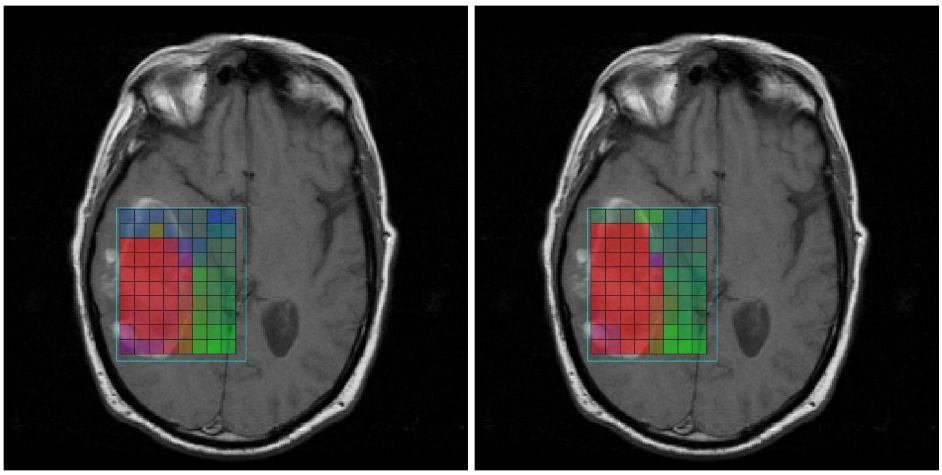

Figure 5. Results show how the surrounding voxels signal values from the PMM (left) have not smoothed the values assigned to each voxel with a larger region of homogeneous voxels compared to the same region of voxels in the SMM (right). Manual analysis of the MV-MRS spectra and the related MRI scan tells of a contrast enhanced ring around the core of the tumour and, thus, is without doubt, high grade tumour tissue and most likely necrotic in the top voxels. Furthermore the manual analysis confirms that the results from the SMM shows a more accurate depiction, per voxel, of the scan than the PMM.

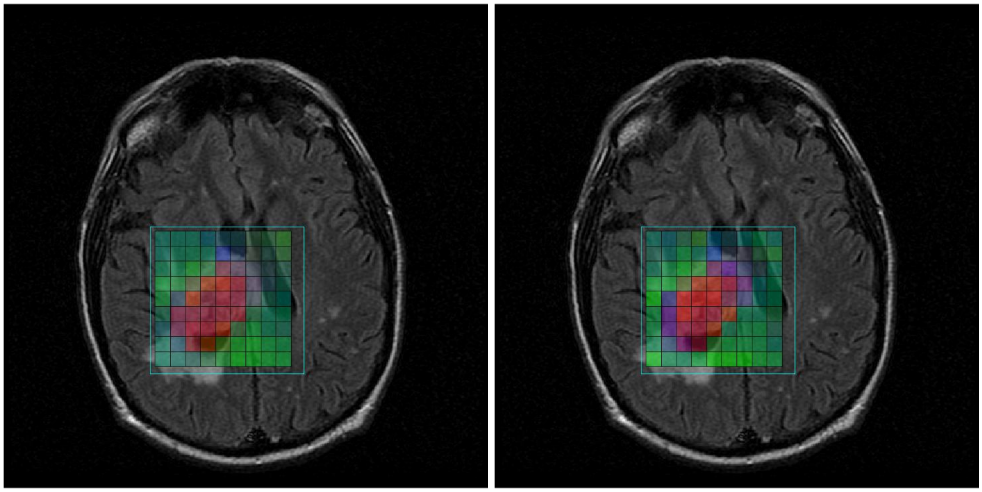

Figure 6. Results show the PMM (left) lessening the strength of the boundaries between the normal and low grade tumour tissue compared to that from the SMM (right), from visual inspection of the MV-MRS data the voxels along the bottom left corner of the scan are known to be normal tissue. The PMM results do show the voxels as mostly normal tissue but with small weighting towards low grade tumour for the same region that the SMM looks more normal. Both maps can be considered as fairly similar.

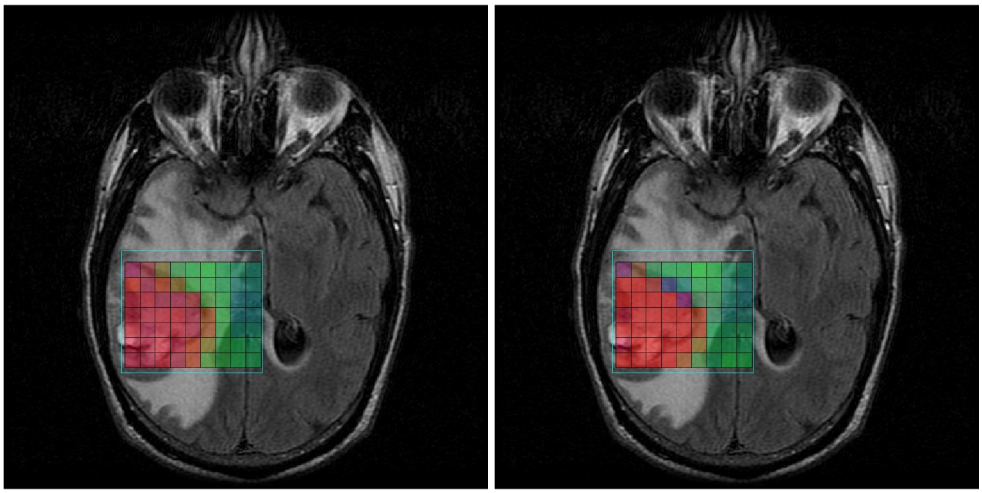

Figure 7. Results show the PMM (left) providing clearer defined boundaries for the high grade tissue to normal tissue found within the scan compared to that of the SMM (right). As with Figure 4 it is unknown as to whether the tissue within the image is fully homogeneous in the regions that the models have predicted so, however having stronger defined boundaries may be a benefit when attempting to determine the centre of a tumour.

4. CONCLUSIONS

In summary this paper presents a novel supervised, spatially aware, Pairwise Mixture Model (PMM) technique for the characterisation of brain tumour tissue into either normal, low (infiltrative) or high (necrotic) grade, from MV-MRS signals to address the problem of the Partial Volume Effect (PVE). The results from testing on a patient dataset showed that when incorporating the information from neighbouring voxels, to add a spatial context, the PMM achieved a higher level of accuracy for classifying tumours into either low grade or high grade than the previous state-of-the-art Signal Mixture Model (SMM). From the results it can be interpreted that the use of the neighbourhood information to help smooth the predictions on the weight coefficients helped to increase the overall classification accuracy. The increased performance from the PMM shows the need for more research into utilising the spatial context when modelling brain tissue. The insights provided by the weight/mixture coefficients when seen as the amount of each tissue type found within a voxel, along with the heatmap graphs, shows the potential for CAD methods such as PMM to be able to replace biopsies in the future.

This paper has shown the advantage of exploiting the spatial context in addressing the partial volume effect in MRS images of brain tumours. Further research must be conducted into utilizing the spatial context within the PMM such as comparison to other methods and more detailed evaluation of the resultant nosological images. Finding the most effective neighbourhood influence size for use within the PMM optimisation, to produce a general model, has potential for not only improving the accuracy of the PMM but in understanding MV-MRS imaging. Future research also provides the opportunity to look at multi-modal, medical imaging, CAD by incorporating the MRI imagery from the outputted heatmap visualizations to the PMM. One method in which to apply this multi-modal approach is by performing a segmentation of an MRI image and mapping the segments with the MV-MRS voxels so as to determine a more relative neighbourhood shape and size for each voxel when applying the PMM optimisation.

REFERENCES

[1] American Brain Tumor Association, “Brain Tumor Statistics.” http://www.abta.org/about-us/news/brain-tumor-statistics/. (Accessed: 10 January 2017).

[2] National Institute for Health and Care Excellence, "Brain cancers overview." https://pathways.nice.org.uk/pathways/brain-cancers. (Accessed: 10 January 2017).
[3] Zacharaki, E. I., Wang, S., Chawla, S., Soo Yoo, D., Wolf, R., Melhem, E. R., and Davatzikos, C., "Classification of brain tumor type and grade using mri texture and shape in a machine learning scheme," *Magnetic resonance in medicine* **62**(6), 1609–1618 (2009).
[4] Yang, G., Raschke, F., Barrick, T. R., and Howe, F. A., "Manifold learning in mr spectroscopy using nonlinear dimensionality reduction and unsupervised clustering," *Magnetic resonance in medicine* **74**(3), 868–878 (2015).
[5] Grant, R., "Overview: brain tumour diagnosis and management/royal college of physicians guidelines," *Journal of Neurology, Neurosurgery & Psychiatry* **75**(suppl 2), ii18–ii23 (2004).
[6] Linck, P., Priedane, E., Hughes, D., and Edwards, R., "Improving outcomes for people with brain and other cns tumours: Analysis of the potential economic impact of the guidance.," (2006).
[7] McGirt, M. J., Woodworth, G. F., Coon, A. L., Frazier, J. M., Amundson, E., Garonzik, I., Olivi, A., and Weingart, J. D., "Independent predictors of morbidity after image-guided stereotactic brain biopsy: a risk assessment of 270 cases," *Journal of neurosurgery* **102**(5), 897–901 (2005).
[8] Malone, H., Yang, J., Hershman, D. L., Wright, J. D., Bruce, J. N., and Neugut, A. I., "Complications following stereotactic needle biopsy of intracranial tumors," *World neurosurgery* **84**(4), 1084–1089 (2015).
[9] Howe, F. A. and Opstad, K. S., "1h mr spectroscopy of brain tumours and masses," *NMR in Biomedicine* **16**(3), 123–131 (2003).
[10] Andrew, E. R., "Nuclear magnetic resonance," *Nuclear Magnetic Resonance, by ER Andrew, Cambridge, UK: Cambridge University Press, 2009* (2009).
[11] Edelman, R. R. and Warach, S., "Magnetic resonance imaging," *New England Journal of Medicine* **328**(10), 708–716 (1993).
[12] Gujar, S. K., Maheshwari, S., Björkman-Burtscher, I., and Sundgren, P. C., "Magnetic resonance spectroscopy," *Journal of neuro-ophthalmology* **25**(3), 217–226 (2005).
[13] Soares, D. and Law, M., "Magnetic resonance spectroscopy of the brain: review of metabolites and clinical applications," *Clinical radiology* **64**(1), 12–21 (2009).
[14] De Vos, M., Laudadio, T., Simonetti, A., Heerschap, A., and Van Huffel, S., "Fast nosologic imaging of the brain," *Journal of Magnetic Resonance* **184**(2), 292–301 (2007).
[15] Luts, J., Laudadio, T., Idema, A. J., Simonetti, A. W., Heerschap, A., Vandermeulen, D., Suykens, J. A., and Van Huffel, S., "Nosologic imaging of the brain: segmentation and classification using mri and mrsi," *NMR in Biomedicine* **22**(4), 374–390 (2009).
[16] De Edelenyi, F. S., Simonetti, A., Postma, G., Huo, R., and Buydens, L., "Application of independent component analysis to 1 h mr spectroscopic imaging exams of brain tumours," *Analytica Chimica Acta* **544**(1), 36–46 (2005).
[17] Wright, A. J., Fellows, G., Byrnes, T., Opstad, K., McIntyre, D., Griffiths, J., Bell, B., Clark, C., Barrick, T., and Howe, F., "Pattern recognition of mrsi data shows regions of glioma growth that agree with dti markers of brain tumor infiltration," *Magnetic resonance in medicine* **62**(6), 1646–1651 (2009).
[18] Asad, M., Yang, G., and Slabaugh, G., "Supervised partial volume effect unmixing for brain tumor characterization using multi-voxel mr spectroscopic imaging," in [*Biomedical Imaging (ISBI), 2016 IEEE 13th International Symposium on*], 436–439, IEEE (2016).
[19] Yang, G., Raschke, F., Barrick, T. R., and Howe, F. A., "Classification of brain tumour 1 h mr spectra: Extracting features by metabolite quantification or nonlinear manifold learning?," in [*Biomedical Imaging (ISBI), 2014 IEEE 11th International Symposium on*], 1039–1042, IEEE (2014).
[20] Yang, G., Raschke, F., Barrick, T. R., and Howe, F. A., "Nonlinear laplacian eigenmaps dimension reduction of in-vivo magnetic resonance spectroscopic imaging analysis," in [*International Society for Magnetic Resonance in Medicine (ISMRM)*], 1967 (2013).
[21] Ortega-Martorell, S., Lisboa, P. J., Vellido, A., Julià-Sapé, M., and Arús, C., "Non-negative matrix factorisation methods for the spectral decomposition of mrs data from human brain tumours," *BMC bioinformatics* **13**(1), 38 (2012).
[22] Ortega-Martorell, S., Ruiz, H., Vellido, A., Olier, I., Romero, E., Julià-Sapé, M., Martín, J. D., Jarman, I. H., Arús, C., and Lisboa, P. J., "A novel semi-supervised methodology for extracting tumor type-specific mrs sources in human brain data," *PloS one* **8**(12), e83773 (2013).
[23] Raschke, F., Fellows, G. A., Wright, A. J., and Howe, F. A., "1h 2d mrsi tissue type analysis of gliomas," *Magnetic resonance in medicine* **73**(4), 1381–1389 (2015).

[24] De Edelenyi, F. S., Rubin, C., Esteve, F., Grand, S., Decorps, M., Lefournier, V., Le Bas, J.-F., and Remy, C., "A new approach for analyzing proton magnetic resonance spectroscopic images of brain tumors: nosologic images," *Nature medicine* **6**(11), 1287–1289 (2000).
[25] Alonso, J., Bartumeus, F., Isamat, F., Ferrer, I., Vila, F., Ferrer, E., Capdevila, A., and AruÂs, C., "Towards a method for automated classification of 1h mrs spectra from brain tumours," *NMR Biomed* **11**, 177–191 (1998).
[26] Marshall, I., Wardlaw, J., Cannon, J., Slattery, J., and Sellar, R., "Reproducibility of metabolite peak areas in 1h mrs of brain," *Magnetic resonance imaging* **14**(3), 281–292 (1996).
[27] Majós, C., Alonso, J., Aguilera, C., Serrallonga, M., Pérez-Martín, J., Acebes, J. J., Arús, C., and Gili, J., "Proton magnetic resonance spectroscopy (1 h mrs) of human brain tumours: assessment of differences between tumour types and its applicability in brain tumour categorization," *European radiology* **13**(3), 582–591 (2003).
[28] Boogaart, V., Den, A., Howe, F., Rodrigues, L., Stubbs, M., and Griffiths, J., "In vivo31p mrs: absolute concentrations, signal-to-noise and prior knowledge," *NMR in biomedicine* **8**(2), 87–93 (1995).
[29] Ernst, T. and Chang, L., "Elimination of artifacts in short echo time 1h mr spectroscopy of the frontal lobe," *Magnetic resonance in medicine* **36**(3), 462–468 (1996).
[30] Prastawa, M., Bullitt, E., Ho, S., and Gerig, G., "A brain tumor segmentation framework based on outlier detection," *Medical image analysis* **8**(3), 275–283 (2004).
[31] Guo, Y., Ruan, S., Landré, J., and Constans, J.-M., "A sparse representation method for magnetic resonance spectroscopy quantification," *IEEE Transactions on Biomedical Engineering* **57**(7), 1620–1627 (2010).
[32] Bauer, S., Nolte, L.-P., and Reyes, M., "Fully automatic segmentation of brain tumor images using support vector machine classification in combination with hierarchical conditional random field regularization," in [*International Conference on Medical Image Computing and Computer-Assisted Intervention*], 354–361, Springer (2011).
[33] Liu, X., Veksler, O., and Samarabandu, J., "Graph cut with ordering constraints on labels and its applications," in [*Computer Vision and Pattern Recognition, 2008. CVPR 2008. IEEE Conference on*], 1–8, IEEE (2008).
[34] Lafferty, J., McCallum, A., Pereira, F., et al., "Conditional random fields: Probabilistic models for segmenting and labeling sequence data," in [*Proceedings of the eighteenth international conference on machine learning, ICML*], **1**, 282–289 (2001).